Kutinlahti, Veli-Pekka; Lehtovuori, Anu; Viikari, Ville

Analyzing and Optimizing the EIRP of a Phase-Tunable Amplifier-Antenna Array

Published in:
IEEE Journal of Microwaves

DOI:
10.1109/JMW.2022.3207952

Published: 06/01/2023

Document Version
Publisher's PDF, also known as Version of record

IEEE Journal of Microwaves

Received 25 May 2022; revised 8 August 2022; accepted 10 September 2022. Date of publication 6 October 2022; date of current version 6 January 2023.

Digital Object Identifier 10.1109/JMW.2022.3207952

Analyzing and Optimizing the EIRP of a Phase-Tunable Amplifier-Antenna Array

VELI-PEKKA KUTINLAHTI, ANU LEHTOVUORI, AND VILLE VIIKARI (Senior Member, IEEE)

(Regular Paper)

Department of Electronics and Nanoengineering, Aalto University School of Electrical Engineering, 02150 Espoo, Finland

CORRESPONDING AUTHOR: Veli-Pekka Kutinlahti (e-mail: veli-pekka.kutinlahti@aalto.fi).

This work was supported by Business Finland through Project RF Sampo.

ABSTRACT We analyze the performance of an amplifier-antenna array by using separately measured amplifier load-pull data and antenna S-parameters and port-specific radiation patterns. We show that the effective isotropic radiated power (EIRP) of the system can be improved by using phase values which differ from progressive phase shift. Maximum EIRP improvement is 1.1 dB in certain steer directions and over 0.5 dB improvement over a large beamsteering range was measured when compared to using the progressive phase-shift envelope.

INDEX TERMS Phased array antennas, load pull, active phased arrays, phase shifters, beam forming.

I. INTRODUCTION

Increased integration of transmitter systems and ever tightening performance requirements call for new ways to analyze and improve the system operation. Losses and size are minimized by removing non-essential components, such as transmission lines and isolators between antennas and amplifiers, and space for antennas is reduced in favor of other components in mobile devices. Thus, previously negligible non-idealities, such as antenna element coupling, need to be taken into account. Accurate system modeling is required to study what the paradigms of design for these new systems are.

In modern multi-port antennas, tight spacing of antenna elements increases coupling between them. In scanning arrays, coupling is unwanted because of mismatch caused by active impedance, also called antenna cross-talk and scan impedance. Mismatch can cause several problems to the amplifier, such as matching losses, oscillations, distortion, increase in noise figure, or even amplifier breakage. Typically, a minimum requirement for the matching level is set to avoid significant problems, but still the varying reflections caused by the antenna array at the amplifier output can degrade performance of the amplifier well before permanent damage is caused. Limiting this degradation as well as distortion, which can cause signals to leak out of the designated frequency band, is a requirement in future systems.

Lowering the effects of coupling in the antenna is a field of ample research consisting of multiple different techniques. These include e.g., decoupling networks [1], [2], [3], [4], [5], neutralization lines [6], [7], [8], and band-gap structures [9], [10], [11]. The amplifiers themselves being tolerant to mismatch tackle the same problem from the other side of the amplifier-antenna interface [12]. Both of these approaches lead to higher design requirements on the components, and possibly additional components in-between the amplifiers and the antenna array.

In the case of limited ability to affect the specifics of the front-end, signal processing techniques provide some possibilities to lower distortion. Digital predistortion (DPD) adjusts the fed signals by taking into account the behavior of the amplifiers under mismatching conditions [13], [14], [15]. DPD does require sampling of the output signals of the amplifier in order to extract the DPD-model coefficients. This, however, makes the model more robust in a dynamic environment, where antenna coupling causing the distortions can change. As the model constantly samples the output, it can adapt to the new coupling by updating the model coefficients.

Even though coupling in the antenna is usually undesired, there are instances where it can be beneficial. For example, the Doherty power amplifier (DPA) employs two amplifiers to

achieve high efficiency and linearity, and this design has been successfully integrated into a two-port antenna structure [16], [17]. This approach removes the need for a separate power-combining network by using the antenna for that purpose. Other examples of beneficial coupling in antennas include antenna clusters [18], [19], [20] and connected arrays [21], [22], [23], which exploit coupling through novel feeding schemes to improve the bandwidth and the steer range of the arrays.

Whereas DPA integrated on a two-port antenna is an example of power-combining on-antenna, the simple integration of a single amplifier and an antenna is also a good approach to reduce losses. Rather than match both components separately to 50 Ω, active integrated antennas (AIA) are designed by placing the amplifier on the antenna and using the antenna to match the amplifier [24], [25], [26]. This reduces losses, and thus increases efficiency and the output power.

These covered concepts try to improve modern transmitting systems, where integration is a key issue. They are partially exclusive, since, for example, decoupling networks cannot be used with AIAs, and in some instances one might prefer the system to have coupling anyway, like with the antenna cluster. The question then arises of which components the modern transmitting system should be composed of and how should it be driven. Modeling these systems that exhibit coupling between elements is also an important aspect, as the AIA element pattern is affected by power amplifier (PA) non-linearity in a coupled array [27].

To tackle the coupling in future antenna systems, we have introduced a method to determine maximum EIRP in our previous paper [28] using phase tuning for a system with amplifiers connected directly at the inputs of antenna array elements. Compared to methods that lower coupling, decoupling networks, neutralization lines or band-gaps, our method does not require any components in-between amplifier and antenna. This decreases design costs regarding the antenna. In multiport antennas utilizing novel feeding schemes, antenna clusters and connected dipoles, our model can take into account the active reflection coefficient (ARC) of individual elements, which is not originally considered. Our system analysis can be used to further optimize these systems by taking into account the amplifier behavior.

DPA and AIA on the other hand are designed without considering their performance in a highly coupled array. If element-to-element coupling in an array composed of these types of integrated antennas is sufficiently large, the matching of individual amplifiers varies and can degrade the performance. Handling the internal coupling in antenna arrays requires capable modelling and optimization, which our method provides.

DPD is an ample tool for modern communication systems, but it is currently very costly. It also requires constant monitoring of the waves at the amplifier-antenna interface, which our method does not, making our method structurally less complex. Our method is also methodically simpler to implement, requiring only the load-pull measurement of the used amplifier and the standard measurement of antenna S-parameters and patterns, but does not offer all the benefits of DPD. Amplifiers can be designed to be intrinsically more robust to matching changes during operation. Currently all amplifiers without isolators suffer from mismatch caused by active impedance to some degree, and thus could benefit from system analysis.

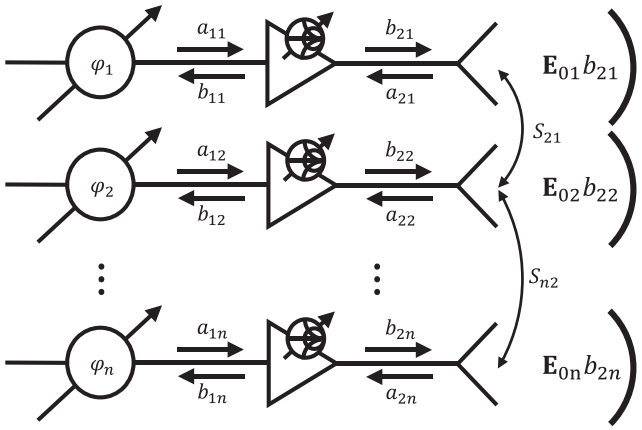

FIGURE 1. Amplifier-antenna system with phase shifters at the inputs of the amplifiers, whose outputs are dependent on reflected waves a_{2i}.

In this paper, we verify our previously published system analysis method to predict accurately the behavior of an amplifier-antenna system. The method utilizes separately measured results of the amplifier load-pull and the antenna array S-parameters and radiation-patterns. We further show, that the system EIRP can be improved in some cases by using phase-shift values not possible with progressive phase shift.

II. SYSTEM MODELING AND OPTIMIZATION

The composition of a general phase-tunable amplifier-antenna array system is presented in Fig. 1, where an n-element antenna array has an amplifier at the port of each antenna element and each amplifier input phase is controlled with an ideal phase shifter. The set comprising a cascaded phase shifter, amplifier, and antenna element is called "a line" in this paper.

The four waves prevalent in the analysis, a_{1i}, a_{2i}, b_{1i} and b_{2i}, are marked in Fig. 1 with their corresponding propagation directions. The wave labels are adopted from amplifier analysis, where a waves are amplifier input waves and b waves are amplifier output waves. Note, that in the case of antennas, a is typically the input wave to the antenna, but in this study the input is the b_{2i} wave. The subscript i denotes the ith element in the system.

Often perfect matching is assumed, i.e., b_1 and a_2 are zero. However, this condition is rarely met in practice and the effect of the waves should be taken into account, as we discuss in the following. However, since the coupling parameters S_{ij} of the antenna array are not zero, the waves will have non-zero values and cause performance degradation of the amplifiers.

The system model was presented in our previous paper [28]. The essential parts of the analysis and the final results are outlined here. The complex output wave b_{2i} of an amplifier is modeled with a function f_{2i}

$$b_{2i} = f_{2i}(|a_{1i}|, a_{2i}e^{-j\varphi_i})e^{j\varphi_i}, \tag{1}$$

where a_{1i} and a_{2i} are the complex input waves of the amplifier input and output, respectively, j is the imaginary unit, and φ_i is the phase of the input wave a_{1i}.The phases of the different waves in the system are with respect to some system level reference, i.e., one of the a_{1i} waves.

In this study, the power P of the input wave a_{1i} is kept constant during the calculation, so we further simplify the expression by taking out the first argument and indexing the function with P as

$$b_{2i} = f_{2i}^{P}(a_{2i}e^{-j\varphi_i})e^{j\varphi_i}. \tag{2}$$

The antenna model is purely linear. It consists of S-parameters, that describe the coupling between the antenna ports, and the far-field electric fields of the elements

$$\mathbf{E}_i = \mathbf{E}_{0i}b_{2i}. \tag{3}$$

We use (2) and the S-parameters of the antenna to find a stable solution for the output of the amplifiers by iteration. After finding the solution, the radiated far-field $\mathbf{E}_{tot}$ is calculated. The system simulation consisting of finding the stable solution of amplifier outputs and final radiated fields using simulated load-pull characteristics and antenna S-parameters are done in MATLAB. Amplifier output solutions solved with MATLAB agree well with simulations performed with the circuit simulation software AWR, where four identical amplifier models are connected with antenna S-parameters, similar to the system in Fig. 1.

The optimization is done with the non-linear optimizer in MATLAB. The used algorithm is the Interior Point Algorithm. The objective function is the EIRP of the system in the steer direction (θ, ϕ)

$$\mathrm{EIRP}(\theta,\phi) = \frac{2\pi r^2|\mathbf{E}_{tot}(\theta,\phi)|^2}{\eta P_{in}} = \frac{2\pi r^2|\sum \mathbf{E}_{0i}(\theta,\phi)b_{2i}|^2}{\eta P_{in}}, \tag{4}$$

where P_{in} is the total power fed into the amplifiers. The EIRP takes into account the outputs b_{2i} of the amplifiers as well as the beam-forming of the antenna array. Thus, the EIRP effectively describes the performance of the whole system in an efficient way.

Maximizing EIRP typically decreases the total power in the a_{2i}-waves, but individual waves might have their power increased. As b_{2i} are affected by the a_{2i}, the optimization needs knowledge of the behavior of the whole system when high coupling is present, which our method provides with simple separate measurements of the amplifier and the antenna array. Other aspects of the system could be added to the optimization objectives and constraints. One important constraint is the requirement for the optimization to reject solutions with unwanted behavior of the amplifiers. Unstable regions of the used amplifier should be avoided. Also, for larger arrays optimizing sidelobe levels might be more beneficial than EIRP optimization.

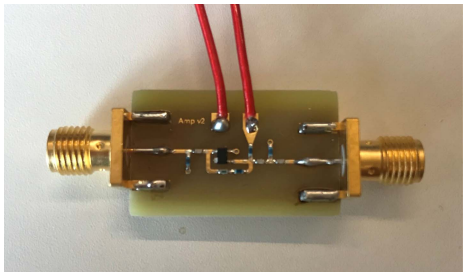

(a)

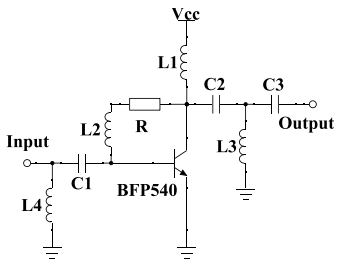

(b)

FIGURE 2. (a) Amplifier prototype manufactured on an FR-4 board, and (b) the schematic of the prototype.

TABLE 1. Component Values of the Amplifier Design.

Component	C1	C2	C3	R
Value	0.9 pF	2 pF	0.7 pF	5.6 kΩ
Component	L1	L2	L3	L4
Value	51 nH	51 nH	1.9 nH	5.1 nH

III. COMPONENT PROTOTYPES

Next, the used BJT-amplifier and the four-element patch antenna are introduced. The information necessary to perform the system analysis with the previously described method is given.

A. AMPLIFIER PROTOTYPE

The amplifier used in this study is a simple BJT common-collector class A amplifier designed on a 1.6-mm thick FR-4 substrate with an Infineon BFP540 transistor. The amplifier is designed in the traditional way to have maximum power to the load P_L when connected to a 50-Ω load at 2.5 GHz. Fig. 2 shows the manufactured amplifier prototype and the schematic of the design with component values in Table 1.

The amplifier is characterized with active load-pull measurements by HITECH from the Netherlands. The characterization is done at 2, 2.25, 2.5, 2.75 and 3 GHz at input powers from −10 to 10 dBm in 1 dBm steps. The magnitude of the output reflection coefficient $|\Gamma_{out}|$ at the fundamental

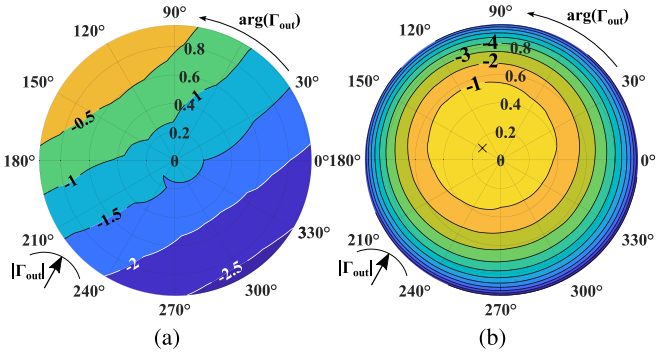

FIGURE 3. Measured load-pull characteristics of the amplifier model averaged over 5 measured prototypes with input power of −10 dBm. (a) $|b_2|$ in dB with respect to Γ_{out} normalized to the maxima, and (b) P_L in dB with respect to Γ_{out} normalized to the maxima.

harmonic is between 0 and 1.2 and between 0 and 1 at the second harmonic.

The measurements are made over a very wide range of values. The measurement results are averaged out, and the analysis of the system is done with the averaged data. The system measurements are made with identically manufactured amplifiers, and the ones that are load-pull measured individually are not used.

Fig. 3 shows the averaged normalized $|b_2|$ and P_L at −10 dBm input power of the individually measured prototypes with respect to output reflection coefficient of the amplifier Γ_{out}. The results in the figure are the average of the five identically manufactured prototypes that are measured with active load-pull, without being connected to the system used in the final results. The design objective is met quite well with the maximum P_L being off by a distance of less than 0.2 from the center in the upper left-quadrant. The gain is 10 dB at 2.5 GHz.

We can see that the amplifier output is very dependent on the phase of Γ_{out}. If $(|\Gamma_{out}|, \arg(\Gamma_{out})) = (0.3, 315)$, $|b_2|$ is over 0.5 dB lower than when the phase is increased by 180°. Therefore, the output of the amplifier can be "phase-tuned" by just adding a length of transmission line to the output.

B. ANTENNA ARRAY PROTOTYPE

The dimensions of the array are chosen so that the coupling between elements is sufficiently high to bring forth the load-dependent effects of the amplifier. The used antenna is a square-patch array designed on a Rogers-4350B substrate, with material parameters $\epsilon_r = 3.66$ and $\tan\delta = 0.0031$. The patches are fed with a probe feeding through the ground plane with SMA connectors. The dimensions of the antenna and substrate are shown in Fig. 4 along with the manufactured prototype. The element and the array are designed with CST Microwave Studio.

Fig. 5 shows the radiation patterns of single elements in the array over the upper hemisphere as well as the S-parameters of the array. The element matching is better than −10 dB at

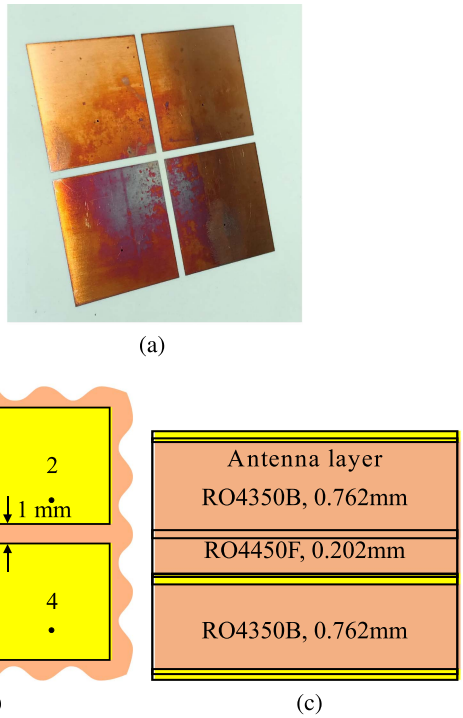

FIGURE 4. (a) Manufactured antenna prototype, (b) the array geometry, with ground plane edge length of 123.2 mm and element spacing 0.26λ at 2.5 GHz, and (c) the substrate stackup.

2.5 GHz and maximum coupling between elements is −7 dB. Assuming equal amplitude in antenna feeding weights, the maximum amplitude of the ARC is over 1, which is obviously very high for a small array and assumes that the phases are intentionally chosen to maximize |ARC|.

The maximum |ARC| of over 1 is, however, not a realistic situation considering that phases φ_i making the far-field pattern utterly unusable would be required. The high coupling here is used to simulate the magnitude of coupling in large antenna arrays, where the total coupling for a single element might raise high from multiple adjacent elements.

IV. SIMULATION RESULTS AND MEASUREMENT SETUP

A. MEASUREMENT SETUP

The antenna patterns and the amplifier-antenna system EIRP are measured with the StarLab measurement system, shown in Fig. 6(a). StarLab measures the full spherical near field of the device under test (DUT) by quickly scanning the multiple probes, placed inside the orange loop visible in the figure, and rotating the DUT. The far field is then calculated from the near field. It is typically used to measure single feed antennas or elements of an array, but system measurements can be done with auxiliary equipment.

The amplifier-antenna system is located in the center of StarLab. The used measurement setup is illustrated in Fig. 6(b). The studied system is the amplifiers and the antenna array that are connected with SMA adapters. A power divider, phase shifters and attenuators are used to control the system. Since the incoming waves $\mathbf{a}_1$ in Fig. 1 are supposed to have

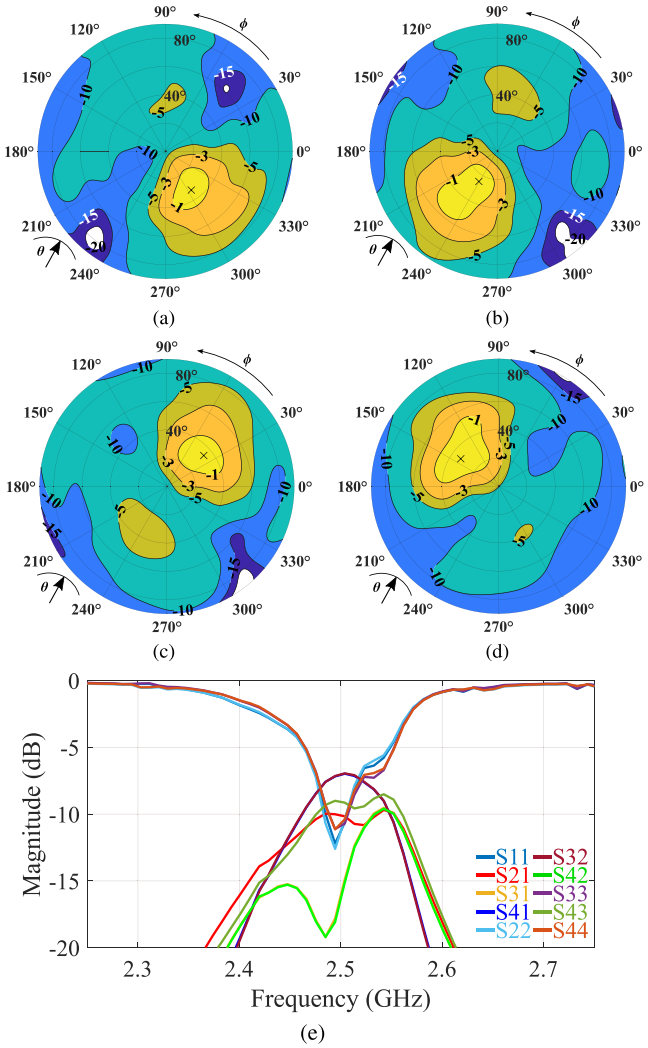

FIGURE 5. **(a)–(d) Normalized measured radiation patterns in dB of elements 1 to 4, respectively, and (e) the measured S-parameters of the manufactured array.**

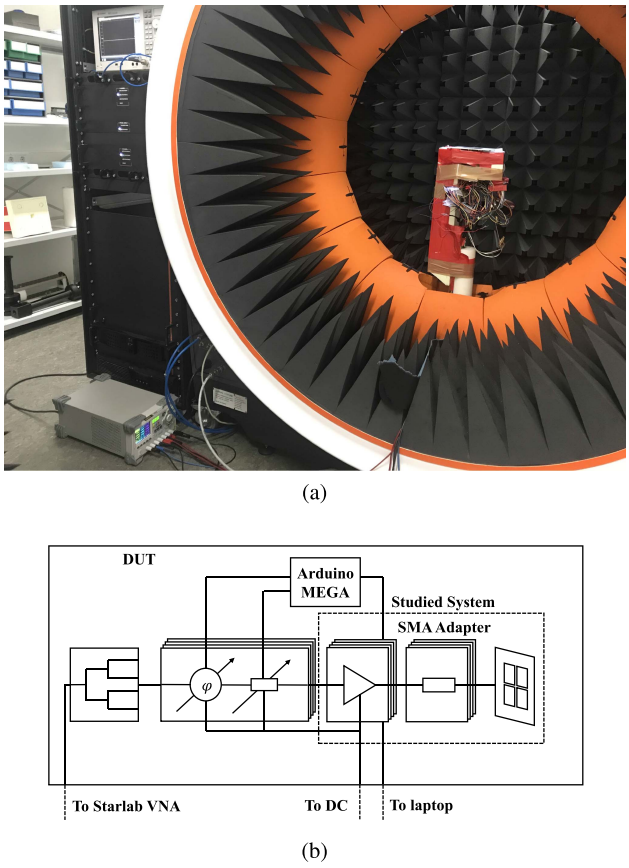

FIGURE 6. **(a) Measurement setup in StarLab. The DC supply for the amplifiers and control circuits is in the lower left corner. (b) Measurement setup block diagram.**

the same non-varying amplitude, the non-ideal phase shifters are combined with attenuators to ensure a more equal power across phase shifting states. The phase shifters attenuate the signals more with increasing phase shift, which is compensated by decreasing the attenuation of the attenuators. The phase shifters and attenuators are controlled with an Arduino MEGA 2056 with a serial monitor via a USB.

The phase shifters and attenuators are behind the amplifiers. Phase shifters and attenuators use, respectively, 6- and 7-bit parallel interfaces, that are controlled with the Arduino. Hence, the 52 cables needed in the measurement setup between the Arduino and phase shifters and attenuators.

B. SIMULATION RESULTS

The system operation is analyzed (2)–(4) by combining the measured load-pull data of the amplifiers with the measured S-parameters and radiation patterns of the antennas. The operation of the combined system is also measured. The results are used to validate the accuracy and usability of proposed method in system behavioral analysis as well as to calculate the optimized phases that maximize the EIRP.

Fig. 7 shows the simulated result for the optimized EIRP envelope, i.e., the largest EIRP values attained over all phase shifts configurations, normalized to the EIRP envelope obtained with the progressive phase shift. Normalization is done to every direction individually. In the −3-dB steer range of the reference, the optimization improves the EIRP at the edges of the steer range, with the maximum being over 0.5 dB. The improvement is minor at the edges of the H-plane, sligthly exceeding 0.1 dB, and the more noticeable improvement is in the E-plane.

Typical antenna arrays utilizing phase shift require additional phase error correction to achieve peak performance. Our algorithm however finds regularly solutions with over 30° phase adjustments, that out perform progressive phase shift with respect to EIRP. These solutions are quick to find in MATLAB using our system model. Finding them with brute force trial-and-error by measuring the system multiple times would increase the time to find the solution tremendously.

The improvement of the EIRP in this type of system is generally only possible for tightly coupled arrays, as

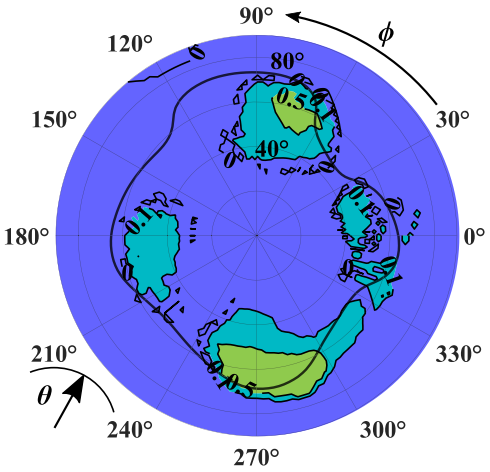

FIGURE 7. Simulated optimized EIRP envelope normalized to the EIRP envelope of progressive phase shift at each direction individually. The −3-dB steer range of the reference is marked with the black line.

unchanging ARC causes the behavior of the amplifiers to be independent of each other. The level of coupling at which this analysis can bring forth improvements for a specific amplifier is unknown at the moment. ARC can also be negated with isolators, but these introduce losses.

V. MEASUREMENT RESULTS

Fig. 8(a) shows the normalized results of the measured EIRP using the progressive phase shift. The measured beam steering directions are marked in the figure, and the values between the measurements closest to the measured direction are used. The simulation in Fig. 8(b) is done with 2° steer resolution, whereas the measurement is only conducted on the E- and H-planes and the two diagonals, that is, with 45° steps in ϕ. The θ-angle resolution in measurement is 12°.

In Fig. 8(c) is the difference plot of Figs. 8(a) and 8(b), and it can be seen that in $\theta = [0°, 270°]$ the error between measurement and simulation is mostly between −0.5 dB and 0.5 dB. In $\theta = [270°, 360°]$ region the measured EIRP is consistently more than 0.5 dB lower than the simulated result. This is probably due to the one amplifier performance greatly deviating from the averaged model used to calculate the simulated behavior. In simulations, the four amplifiers are identical, whereas the amplifiers used in the system measurements, the performance of the amplifiers was not meticulously validated.

The same results are plotted for the envelopes in Fig. 9(a)–(c). In Fig. 9(c) it can be seen, that the areas pointed for Fig. 8(c) are behaving similarly. In $\theta = [0°, 270°]$ and $\phi < 60°$ the difference is quite nicely between −0.5 dB and 0.5 dB, whereas in $\theta = [270°, 360°]$ the measurement drops below −1 dB compared to the simulated result.

Generally, the measurement accuracy of antenna patterns is within 0.5 dB with the StarLab. Our model consists of additional inaccuracies because of the amplifier model. This

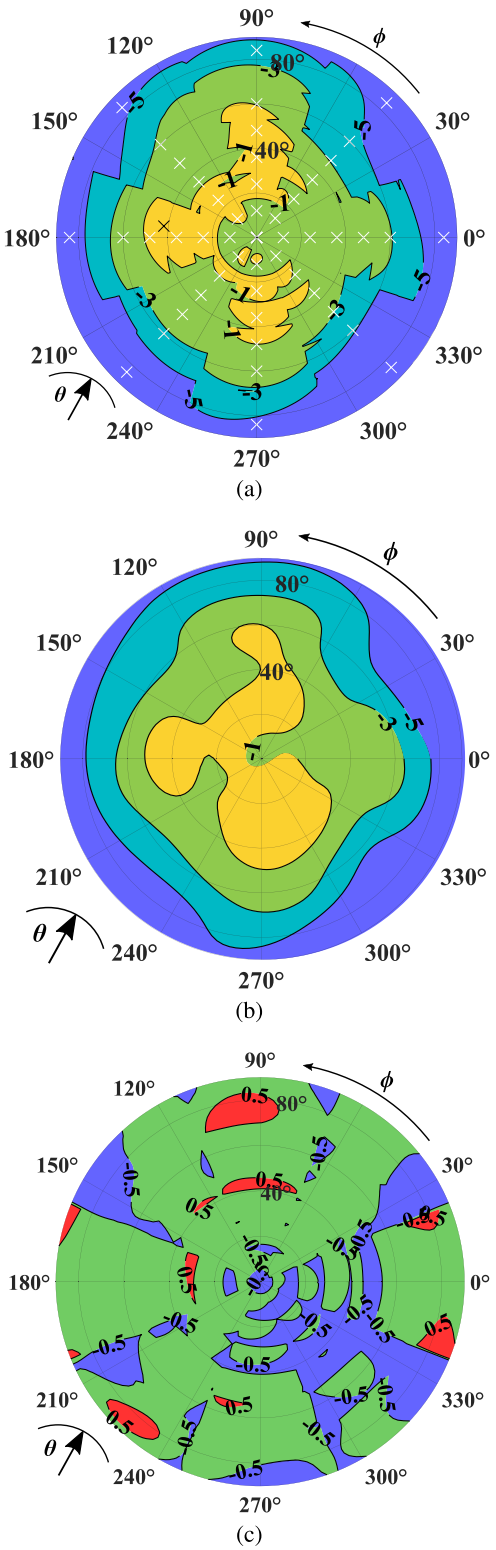

FIGURE 8. (a) EIRP of the measured system in dB using progressive phase shift normalized to the maxima. The measured steer directions are marked with white, crosses, and values to the directions between the points are taken from the measurement with steer direction closest to the direction. (b) Simulated EIRP of the progressive phase shift using measured component models normalized to the maxima. (c) The difference between measured and simulated results.

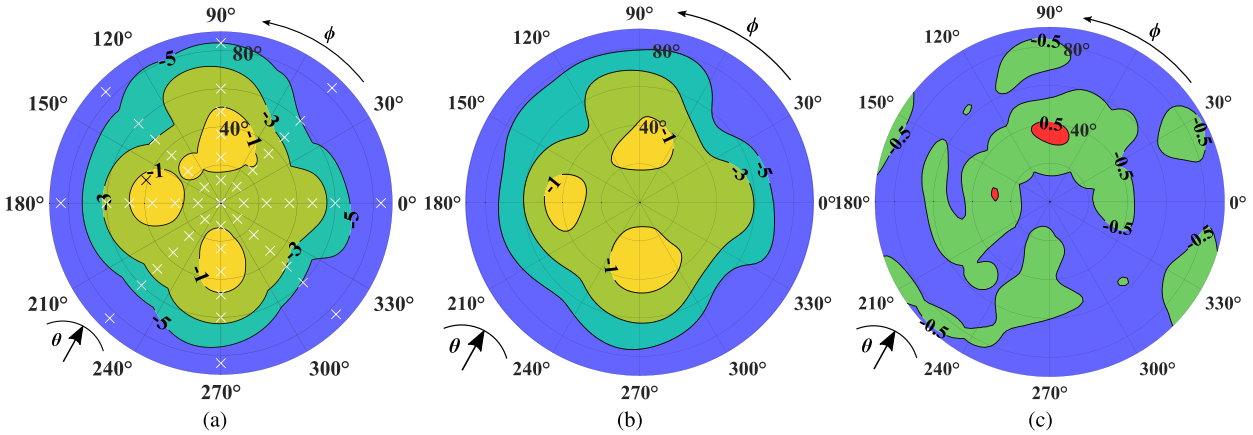

FIGURE 9. (a) EIRP envelope of the measured system in dB using progressive phases normalized to the maxima. The measured steer directions are marked with white crosses. (b) Simulated EIRP envelope in dB obtained with the progressive phase shift normalized to the maxima. (c) The difference between measured and simulated results.

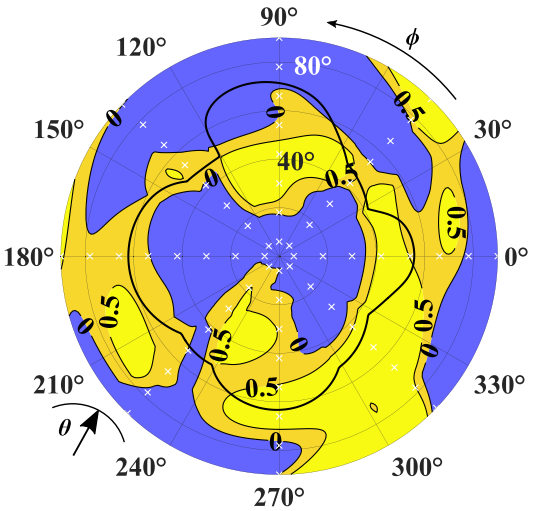

FIGURE 10. EIRP envelope of the measured system using optimized phases normalized to the measured reference envelope at each direction individually. The measured steer directions are marked with white crosses. The black line marks the −3-dB steer range of the reference envelope.

is a consequence of the fact that the average model was used instead of individual load-pull measurements of each amplifier.

Fig. 10 shows the improvement of the measured EIRP using the optimized phases. An improvement of over 0.5 dB is achieved across large angular areas, the maximum improvement being 1.1 dB at $(\theta, \phi) = (30^\circ, 105^\circ)$. There is, however, a large area where the EIRP decreases in the center of the plot. The maximum decrease is at $(\theta, \phi) = (20^\circ, 0^\circ)$, being -1.5 dB and being quite precisely at a measurement point.

Although there are differences in the measured results compared to simulated ones, the results demonstrate that improvement in the EIRP can be achieved with optimized feeding coefficients. However, reliable prediction of performance requires accurate models and careful manufacturing. The measurement procedures should be developed as well. The simulations are done with 2° beam steering resolution, which corresponds to 8280 steer directions, whereas the measurements are done in 49 directions. Thus, the measurements should have been concentrated in the areas where improvement is to be expected and not to cover the entire steer area. These aspects will have a key role to guarantee the high performance in future wireless systems and will offer important research topics.

VI. CONCLUSION

We have shown, that our system-level simulations of an amplifier-antenna system predict the EIRP accurately. The model uses separate measurements of the amplifier and the antenna array to predict the system behavior. We have also shown, that the EIRP of the system can be improved by using non-conventional steering phases. The system EIRP improved by 0.5 dB as compared to the reference case over large areas of the −3-dB steer range, with the maximum being 1.1 dB.

REFERENCES

[1] Y.-F. Cheng and K.-K. M. Cheng, "Compact wideband decoupling and matching network design for dual-antenna array," *IEEE Antennas Wireless Propag. Lett.*, vol. 19, no. 5, pp. 791–795, May 2020.

[2] X.-J. Zou, G.-M. Wang, Y.-W. Wang, and H.-P. Li, "An efficient decoupling network between feeding points for multielement linear arrays," *IEEE Trans. Antennas Propag.*, vol. 67, no. 5, pp. 3101–3108, May 2019.

[3] Y.-M. Zhang and S. Zhang, "A novel aperture-loaded decoupling concept for patch antenna arrays," *IEEE Trans. Microw. Theory Techn.*, vol. 69, no. 9, pp. 4272–4283, Sep. 2021.

[4] S.-W. Su, C.-T. Lee, and Y.-W. Hsiao, "Compact two-inverted-F-antenna system with highly integrated π-shaped decoupling structure," *IEEE Trans. Antennas Propag.*, vol. 67, no. 9, pp. 6182–6186, Sep. 2019.

[5] Y.-M. Zhang, Q.-C. Ye, G. F. Pedersen, and S. Zhang, "A simple decoupling network with filtering response for patch antenna arrays," *IEEE Trans. Antennas Propag.*, vol. 69, no. 11, pp. 7427–7439, Nov. 2021.

[6] R. Liu, X. An, H. Zheng, M. Wang, Z. Gao, and E. Li, "Neutralization line decoupling tri-band multiple-input multiple-output antenna design," *IEEE Access*, vol. 8, pp. 27018–27026, 2020.

[7] M. Li, L. Jiang, and K. L. Yeung, "A general and systematic method to design neutralization lines for isolation enhancement in MIMO antenna arrays," *IEEE Trans. Veh. Technol.*, vol. 69, no. 6, pp. 6242–6253, Jun. 2020.

[8] W. Hu et al., "Dual-band ten-element MIMO array based on dual-mode IFAs for 5G terminal applications," *IEEE Access*, vol. 7, pp. 178476–178485, 2019.

[9] X. Shen, Y. Liu, L. Zhao, G.-L. Huang, X. Shi, and Q. Huang, "A miniaturized microstrip antenna array at 5G millimeter-wave band," *IEEE Antennas Wireless Propag. Lett.*, vol. 18, no. 8, pp. 1671–1675, Aug. 2019.

[10] H. N. Chen, J.-M. Song, and J.-D. Park, "A compact circularly polarized MIMO dielectric resonator antenna over electromagnetic band-gap surface for 5G applications," *IEEE Access*, vol. 7, pp. 140889–140898, 2019.

[11] P. Sambandam et al., "Compact monopole antenna backed with fork-slotted EBG for wearable applications," *IEEE Antennas Wireless Propag. Lett.*, vol. 19, no. 2, pp. 228–232, Feb. 2020.

[12] C. R. Chappidi, T. Sharma, and K. Sengupta, "Multi-port active load pulling for mm-wave 5G power amplifiers: Bandwidth, back-off efficiency, and VSWR tolerance," *IEEE Trans. Microw. Theory Techn.*, vol. 68, no. 7, pp. 2998–3016, Jul. 2020.

[13] K. Hausmair, P. N. Landin, U. Gustavsson, C. Fager, and T. Eriksson, "Digital predistortion for multi-antenna transmitters affected by antenna crosstalk," *IEEE Trans. Microw. Theory Techn.*, vol. 66, no. 3, pp. 1524–1535, Mar. 2018.

[14] Q. Zhang, W. Chen, and Z. Feng, "Reduced cost digital predistortion only with in-phase feedback signal," *IEEE Microw. Wireless Compon. Lett.*, vol. 28, no. 3, pp. 257–259, Mar. 2018.

[15] N. Guan, N. Wu, and H. Wang, "Model identification for digital predistortion of power amplifier with signed regressor algorithm," *IEEE Microw. Wireless Compon. Lett.*, vol. 28, no. 10, pp. 921–923, Oct. 2018.

[16] O. A. Iupikov et al., "A cavity-backed patch antenna with distributed multi-port feeding, enabling efficient integration with Doherty power amplifier and band-pass filter," *IEEE Trans. Antennas Propag.*, vol. 69, no. 8, pp. 4412–4422, Aug. 2021.

[17] O. A. Iupikov et al., "A dual-fed PIFA antenna element with non-symmetric impedance matrix for high-efficiency Doherty transmitters: Integrated design and OTA-characterization," *IEEE Trans. Antennas Propag.*, vol. 68, no. 1, pp. 21–32, Jan. 2020.

[18] J.-M. Hannula, T. Saarinen, J. Holopainen, and V. Viikari, "Frequency reconfigurable multiband handset antenna based on a multichannel transceiver," *IEEE Trans. Antennas Propag.*, vol. 65, no. 9, pp. 4452–4460, Sep. 2017.

[19] R. Luomaniemi, J.-M. Hannula, R. Kormilainen, A. Lehtovuori, and V. Viikari, "Unbroken metal rim MIMO antenna utilizing antenna clusters," *IEEE Antennas Wireless Propag. Lett.*, vol. 18, no. 6, pp. 1071–1075, Jun. 2019.

[20] R. Luomaniemi, P. Ylä-Oijala, A. Lehtovuori, and V. Viikari, "Designing hand-immune handset antennas with adaptive excitation and characteristic modes," *IEEE Trans. Antennas Propag.*, vol. 69, no. 7, pp. 3829–3839, Jul. 2021.

[21] M. Ikram, E. A. Abbas, N. Nguyen-Trong, K. H. Sayidmarie, and A. Abbosh, "Integrated frequency-reconfigurable slot antenna and connected slot antenna array for 4G and 5G mobile handsets," *IEEE Trans. Antennas Propag.*, vol. 67, no. 12, pp. 7225–7233, Dec. 2019.

[22] Y. Li, S. Xiao, C.-H. Hu, and Z. Yao, "A low-profile light-weight wideband connected parallel slot array for wide-angle scanning," *IEEE Trans. Antennas Propag.*, vol. 68, no. 2, pp. 813–823, Feb. 2020.

[23] P. Khanal, J. Yang, M. Ivashina, A. Höök, and R. Luo, "A wide scanning array of connected bowtie antennas suitable for integration in composite sandwich structures with Monte-Carlo tolerance analysis," *IEEE Access*, vol. 9, pp. 146691–146702, 2021.

[24] W.-C. Liao, R. Maaskant, T. Emanuelsson, V. Vassilev, O. Iupikov, and M. Ivashina, "A directly matched PA-integrated *K*-band antenna for efficient mm-wave high-power generation," *IEEE Antennas Wireless Propag. Lett.*, vol. 18, no. 11, pp. 2389–2393, Nov. 2019.

[25] Y. Lu et al., "Seamless integration of active antenna with improved power efficiency," *IEEE Access*, vol. 8, pp. 48399–48407, 2020.

[26] F. Zubir, P. Gardner, M. K. A. Rahim, O. Ayop, and N. A. Samsuri, "Analytical solution of amplifier-antenna system's impedance matching requirement for reliable microwave transmitter," *IEEE Access*, vol. 8, pp. 182640–182662, 2020.

[27] A. R. Vilenskiy et al., "Co-design and validation approach for beam-steerable phased arrays of active antenna elements with integrated power amplifiers," *IEEE Trans. Antennas Propag.*, vol. 69, no. 11, pp. 7497–7507, Nov. 2021.

[28] V.-P. Kutinlahti, A. Lehtovuori, and V. Viikari, "Amplifier-antenna array optimization for EIRP by phase tuning," in *Proc. 16th Eur. Conf. Antennas Propag.*, 2022, pp. 1–5.